CrossMark

Structural and functional studies of a metallo-β-lactamase unveil a new type of structurally encoded nickel-containing heterodinuclear site

Hwajung Choi,[a]‡ Hee Jung Kim,[b]‡ Atsushi Matsuura,[b]‡ Bunzo Mikami,[c] Hye-Jin Yoon[a] and Hyung Ho Lee[a]*

[a]Department of Chemistry, College of Natural Sciences, Seoul National University, Seoul 151-742, Republic of Korea, [b]Department of Bio and Nano Chemistry, Kookmin University, Seoul 136-702, Republic of Korea, and [c]Laboratory of Quality Design and Exploitation, Division of Agronomy and Horticultural Science, Graduate School of Agriculture, Kyoto University, Kyoto 611-0011, Japan. *Correspondence e-mail: hyungholee@snu.ac.kr

The selection of correct metal ions with high fidelity against competing cellular cations is crucial for the function of many metalloenzymes; however, the understanding of the principles that govern metal selectivity is still incomplete. In this study, the crystal structure of the Tm1162 protein from *Thermotoga maritima*, a metallo-β-lactamase, is reported. Several crystal structures of wild-type Tm1162 and its mutants were solved. Homologues of Tm1162 are widely distributed in bacteria and archaea, including several human pathogens. The monomer possesses an $\alpha\beta/\beta\alpha$ fold, with the core β-strands having the β-sheet sandwich structure common to the metallo-β-lactamase superfamily. Tm1162 exists as a trimer in the crystal and this trimeric unit is likely to be present in solution. In the trimer, three active sites reside at the interface between subunits, suggesting that the oligomeric assembly is crucial for catalysis. A new type of structurally encoded heterodinuclear site has been identified by confirming the identity of nickel-containing heteronuclear sites in Tm1162 *via* X-ray absorption spectroscopy and anomalous difference Fourier maps. The second coordination sphere, including His8 and Glu73, maintains the side-chain orientations of histidines and stabilizes the metal-binding site. Nickel coordination was crucial for the oligomerization of Tm1162. The nickel-dependent and manganese-dependent β-lactamase and phosphodiesterase activities of Tm1162 have also been characterized.

1. Introduction

Metal ions are essential components of many proteins and play a crucial role in protein functions. As cellular fluids contain a mixture of metals at varying concentrations, it is important to understand the principles that govern protein–metal interactions (Dudev & Lim, 2014). To address this issue, it is necessary to determine the atomic structure of protein–metal complexes and to analyze the detailed interactions between them. In an attempt to identify a new class of heterodinuclear metal sites in the metallo-β-lactamase superfamily, we have determined the crystal structure of the Tm1162 protein from *Thermotoga maritima*. Homologues of Tm1162 are widely distributed in bacteria and archaea, including several human pathogens. It is classified as a UPF0173 metal-dependent hydrolase in the UniProtKB/Swiss-Prot database (The UniProt Consortium, 2013) and is predicted to belong to the metallo-β-lactamase (MBL) superfamily in the Pfam database (PF00753; Neuwald *et al.*,
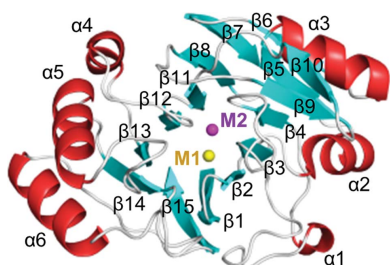
1997; Punta *et al.*, 2012). In the hydrolysis reactions catalyzed by metallo-β-lactamases, a metal-activated hydroxide ion serves as a critical nucleophile (Christianson & Cox, 1999).

Antibiotics containing the β-lactam moiety are some of the major antimicrobial agents used today; however, the emergence of antibiotic-resistant pathogens is a significant public health concern (Feng *et al.*, 2014; Palzkill, 2013). The most common cause of resistance to β-lactam-containing antibiotics is the expression of β-lactamases capable of catalyzing the hydrolysis of the β-lactam moiety, thus providing bacteria with resistance against β-lactam antibiotics (Pérez-Llarena & Bou, 2009). β-Lactamases have attracted much attention as a target for the discovery of antibacterial drugs (Eidam *et al.*, 2012; Fast & Sutton, 2013), as their inhibition would enable the continued use of the widely used β-lactam antibiotics (Bebrone, 2007). They have been categorized into four classes (classes A–D). β-Lactamases in subgroups A, C and D show different substrate specificities, but they share a key serine residue in the active site that plays a crucial role in attacking the β-lactam moiety (Fisher *et al.*, 2005). Class B β-lactamases are distinct from the serine β-lactamases in terms of catalytic mechanism. They require one or two Zn^{2+} ions for their activity and can be divided into three subclasses: B1–B3 (Heinz & Adolph, 2004). The key structural feature of class B2 β-lactamases is that the Zn^{2+} ion is coordinated by three histidine side chains and one cysteine at the active site (Hu *et al.*, 2009; Quiroga *et al.*, 2000). It has also been shown that the zinc-binding site in β-lactamase L1, belonging to class B3, is highly flexible and therefore can accommodate other transition metals, including nickel (Hu *et al.*, 2009). Despite intensive structural studies on many β-lactamases, no nickel-dependent enzyme has been characterized structurally or functionally among the members of the MBL superfamily.

Nickel is an essential nutrient for microorganisms. To incorporate nickel ion into nickel-dependent enzymes, nickel-specific permeases or ATP-binding cassette-type transport systems are used to take up Ni^{2+} (Mulrooney & Hausinger, 2003). At least nine types of nickel-dependent enzyme have been identified through intensive structural and functional studies: urease, NiFe-hydrogenase, carbon monoxide dehydrogenase, acetyl-coenzyme A decarbonylase/synthase, methyl-coenzyme M reductase, Ni-dependent superoxide dismutase, Ni-dependent glyoxylase, acireductone dioxygenase and methylenediurease (Ragsdale, 2009). Nevertheless, additional nickel-dependent enzymes may be discovered, as nickel is widely used as an essential nutrient in microorganisms (Boer *et al.*, 2014).

Here, we report the crystal structures of wild-type Tm1162 and its mutants, together with the results of structure-based mutation analyses, X-ray absorption spectroscopy, anomalous difference Fourier map calculation and enzymatic assays of Ni^{2+}-dependent and Mn^{2+}-dependent phosphodiesterase and β-lactamase activities. This work has revealed the distinct features of the Tm1162 active site and identified a new nickel-dependent metallo-β-lactamase in a microorganism. In the crystal, Tm1162 exists as a trimer and the active sites reside at the interface between two subunits. The second coordination sphere maintains the side-chain orientations of histidines and stabilizes the nickel-containing heterodinuclear site. Nickel coordination is essential for the trimeric oligomerization of Tm1162, and the nickel-dependent and manganese-dependent β-lactamase and phosphodiesterase activities were also characterized.

2. Materials and methods

2.1. Cloning, protein expression and purification

The coding region corresponding to the full-length Tm1162 protein (residues 1–226) from *T. maritima* was amplified by polymerase chain reaction (PCR) using the genomic DNA as a template. The PCR fragments had the correct size on agarose gel electrophoresis and were cloned into the pHis2 parallel expression vector (Sheffield *et al.*, 1999) in the NcoI and NotI sites. Each construct codes for an N-terminal His$_6$ tag, a *Tobacco etch virus* (TEV) protease cleavage site and the *Tm1162* gene under the control of the T7 promoter. The resulting plasmid coding for the *Tm1162* gene was transformed into *Escherichia coli* strain BL21(DE3) Star cells. The overexpression of Tm1162 was induced by the addition of 0.5 mM isopropyl β-D-1-thiogalactopyranoside (IPTG) and the cells were grown at 298 K for 19 h. The cells were lysed by passage through a French press in a lysis buffer consisting of 20 mM Tris–HCl pH 7.9, 500 mM NaCl, 5 mM imidazole, 1 mM phenylmethylsulfonyl fluoride (PMSF). Tm1162 was purified by Ni-Sepharose affinity chromatography (GE Healthcare). The His$_6$ tag was cleaved using TEV protease at 277 K overnight. Tm1162 was further purified by size-exclusion chromatography (HiLoad 16/600 Superdex 200 prep grade, GE Healthcare) and concentrated to 21 mg ml^{-1} by ultrafiltration. The homogeneity of the purified protein was assessed by polyacrylamide gel electrophoresis (PAGE) in the presence of 0.1%(w/v) sodium dodecyl sulfate (SDS). The protein concentration was estimated by measuring the absorbance at 280 nm and employing the calculated molar extinction coefficient of 16 055 M^{-1} cm^{-1} (Swiss-Prot; http://www.expasy.org/).

When overexpressing the selenomethionine (SeMet)-substituted protein in *E. coli* BL21(DE3) cells, we used M9 cell-culture medium that contained extra amino acids including SeMet. Otherwise, the procedure for preparing the SeMet-substituted protein was essentially the same as that described above. Tm1162 mutants (H8A, H48A, H8A/H48A, Y72A and E73A) were purified essentially as described above. Tm1162 in complex with Ni^{2+} was prepared by incubating the apoprotein with Ni^{2+} ions. The Tm1162 apoprotein was prepared by adding a 30-fold excess of EDTA to the protein solution followed by incubation at 4°C overnight. EDTA was removed by using a desalting column against a buffer solution consisting of 50 mM Tris–HCl pH 7.5, 200 mM NaCl. The Tm1162 apoprotein was then metallated with Ni^{2+} by adding NiSO$_4$ (5 mM) to the apoprotein (∼800 μM) followed by incubation at 4°C for 1 h. Further purification was performed by using a desalting column to remove unbound nickel ions.

2.2. Crystallization, X-ray data collection and structure determination

Crystals of SeMet-substituted Tm1162 protein were grown at 293 K using the sitting-drop method by mixing 1 μl Tm1162 solution at 21 mg ml^{-1} in 20 mM Tris–HCl pH 8.0, 200 mM NaCl, 1 mM dithiothreitol (DTT) with 1 μl reservoir solution consisting of 100 mM Tris–HCl pH 8.5, 55%(v/v) 2-methyl-2,4-pentanediol. Single-wavelength anomalous diffraction (SAD) data were collected using 0.9789 Å wavelength X-rays on the BL44XU beamline at SPring-8. Native crystals of Tm1162 diffracted to a resolution of 1.92 Å and the diffraction data were processed and scaled using the *HKL*-2000 software package (Otwinowski & Minor, 1997). The crystal belonged to space group $P32_1$, with unit-cell parameters a = 98.7, b = 98.7, c = 45.3 Å. SAD phasing, solvent-flattening, density modification and partial model building by *RESOLVE* (Terwilliger, 2003) led to an initial model. The model was improved by iterative cycles of manual rebuilding using *Coot* (Emsley & Cowtan, 2004) and refinement using *PHENIX* (Adams *et al.*, 2002). Several rounds of model building, simulated annealing, positional refinement and individual B-factor refinement were performed using *Coot* and *PHENIX*. Table 1 lists the refinement statistics. The atomic coordinates and structure factors of wild-type Tm1162 have been deposited in the Protein Data Bank as PDB entry 3x30.

2.3. Model refinement of wild-type and mutants of Tm1162

Crystals of nickel-complexed Tm1162 were grown at 298 K using the hanging-drop method by mixing 1 μl of a 20 mg ml^{-1} solution of EDTA-treated wild-type Tm1162 in 20 mM Tris–HCl pH 8.0, 200 mM NaCl, 1 mM DTT, 5 mM NiSO$_4$ with 1 μl reservoir solution consisting of 100 mM Tris–HCl pH 8.6, 55%(v/v) 2-methyl-2,4-pentanediol. Crystals of the H8A mutant of Tm1162 were grown at 298 K using the hanging-drop method by mixing 1 μl of a 20 mg ml^{-1} solution of Tm1162 H8A mutant in 20 mM Tris–HCl pH 8.0, 200 mM NaCl, 1 mM DTT with 1 μl reservoir solution consisting of 100 mM Tris–HCl pH 9.2, 51%(v/v) 2-methyl-2,4-pentanediol.

Data sets were collected at 100 K in 1° oscillations on the 5C beamline at Pohang Light Source (PLS). Crystals of wild-type Tm1162 in complex with Ni^{2+} and of the H8A and H48A mutants of Tm1162 diffracted to resolutions of 2.33, 2.67 and 3.30 Å, respectively (Tables 1 and 2), and the diffraction data were processed and scaled using the *HKL*-2000 software package (Otwinowski & Minor, 1997). The structures were solved using the molecular-replacement method using the model of Tm1162 (PDB entry 3x30) as a probe. A cross-rotational search followed by a translational search was performed using *Phaser* (McCoy *et al.*, 2007). Subsequent manual model building was performed using *Coot* (Emsley & Cowtan, 2004) and restrained refinement was carried out using *PHENIX* (Adams *et al.*, 2002). Several rounds of model building, simulated annealing, positional refinement and individual B-factor refinement were performed using *Coot* and *PHENIX*. Tables 1 and 2 list the data-collection and refine-

ment statistics. The atomic coordinates and structure factors of wild-type Tm1162 in complex with Ni^{2+} and of the H8A and H48A mutants of Tm1162 have been deposited in the Protein Data Bank (PDB entries 3x2z, 3x2y and 3x2x, respectively).

2.4. X-ray absorption spectroscopy and nickel anomalous difference maps

Fluorescence scans were performed on crystals of wild-type Tm1162, nickel-complexed Tm1162 and the H8A mutant on the 5C beamline at PLS near the X-ray absorption edge of nickel ions. The anomalous diffraction data were collected at the peak position of the nickel absorption edge (8.351 keV). Anomalous data sets for nickel-complexed Tm1162 crystals and H8A mutant crystals were processed with the *HKL*-2000 software package (Otwinowski & Minor, 1997). Tables 1 and 2 list the anomalous data-collection statistics. Anomalous difference Fourier map calculation was performed using *FFT* in *CCP*4 (Winn *et al.*, 2011).

2.5. Analytical gel filtration

The purified Tm1162 proteins were subjected to analytical gel-filtration chromatography on a Superdex 200 (10/300 GL) column with a running buffer consisting of 20 mM Tris–HCl pH 8.0, 200 mM NaCl at a constant flow rate of 0.5 ml min^{-1}. A standard curve was obtained using molecular-weight markers (Sigma), which included β-amylase, alcohol dehydrogenase, carbonic anhydrase and cytochrome c. The Stokes radii of these markers were calculated from their crystal structures (PDB entries 1fa2, 2hcy, 1v9e and 1hrc, respectively; Cheong *et al.*, 1995; Raj *et al.*, 2014; Saito *et al.*, 2004; Bushnell *et al.*, 1990) using the *HYDROPRO* program (García De La Torre *et al.*, 2000). The Tm1162 apoprotein was prepared by desalting in a buffer consisting of 20 mM Tris–HCl pH 8.0, 200 mM NaCl, 5 mM EDTA. EDTA was then removed by desalting against a buffer solution consisting of 50 mM Tris–HCl pH 7.5. 200 mM NaCl. The Tm1162 apoprotein was metallated by adding each of the metal solutions (1 mM) to the apoprotein ($\sim$800 μM) and incubating the sample at 4°C for 1 h.

2.6. β-Lactamase assay

β-Lactamase activity was measured with the substrate nitrocefin by monitoring the increase in absorbance at 485 nm (owing to the product; Wang & Benkovic, 1998). The assay included 5 μM nitrocefin in a reaction mixture consisting of 1 μM Tm1162, 50 mM HEPES–NaOH pH 7.0. The reactions were performed at 25°C for 20 min. For metal chelation, the Tm1162 protein was purified with a buffer consisting of 20 mM Tris–HCl pH 8.0, 200 mM NaCl with 5 mM EDTA in all buffers during purification and was subsequently desalted by gel filtration in a buffer consisting of 20 mM Tris–HCl pH 8.0, 200 mM NaCl. To determine the K_m and k_{cat} values of Tm1162, the enzyme reactions were initiated by the addition of a concentrated aliquot of Tm1162 to the reaction solution. The final concentration of the Tm1162 protein ranged from 250 nM to 4 μM.

Table 1
Data-collection and refinement statistics for wild-type Tm1162.

Values in parentheses are for the outer shell.

	SeMet derivative, peak	Native, nickel peak	Nickel complex
Crystal parameters			
X-ray source	BL44XU, SPring-8	5C, PLS	5C, PLS
X-ray wavelength (Å)	0.9789	1.4847	1.0000
Space group	$P32_1$	$P4_12_12$	$P4_12_12$
Unit-cell parameters (Å)	$a = b = 98.7$,	$a = b = 143.5$,	$a = b = 143.5$,
	$c = 45.3$	$c = 149.8$	$c = 149.9$
Resolution range (Å)	30–1.92 (1.95–1.92)	50–3.65 (3.71–3.65)	50–2.33 (2.37–2.33)
Total/unique reflections	412656/37623	169483/17984	914034/66863
Completeness (%)	100.0 (100.0)	99.8 (100.0)	99.9 (99.9)
Average $I/\sigma(I)$	50.0 (8.3)	15.8 (6.8)	45.6 (7.6)
R_{merge}† (%)	9.8 (48.3)	21.8 (49.3)	10.5 (52.6)
Model-refinement statistics			
Resolution range (Å)	28.5–1.92		48.07–2.33
R_{work}/R_{free}‡ (%)	15.6/18.2		19.1/20.5
No. of atoms			
Protein non-H atoms	1737		5211
Water O atoms	157		323
Average B factors (Å^2)			
Protein non-H atoms	23.31		34.58
Water O atoms	34.01		40.30
R.m.s. deviations from ideal			
Bond lengths (Å)	0.008		0.004
Bond angles (°)	1.092		0.877
Protein geometry analysis			
Ramachandran favoured (%)	96.89		95.41
Ramachandran allowed (%)	3.11		4.59
Ramachandran outliers (%)	0		0

† $R_{merge} = \sum_{hkl} \sum_i |I_i(hkl) - \langle I(hkl) \rangle| / \sum_{hkl} \sum_i I_i(hkl)$, where $I(hkl)$ is the intensity of reflection hkl, $\sum_{hkl}$ is the sum over all reflections and $\sum_i$ is the sum over i measurements of reflection hkl. ‡ $R = \sum_{hkl} ||F_{obs}| - |F_{calc}|| / \sum_{hkl} |F_{obs}|$, where R_{free} was calculated for a randomly chosen 5% of reflections which were not used for structure refinement and R_{work} was calculated for the remaining reflections.

Table 2
Data-collection and refinement statistics for Tm1162 mutants.

Values in parentheses are for the outer shell.

	H8A	H8A, nickel peak	H48A
Crystal parameters			
X-ray source	5C, PLS	5C, PLS	7A, PLS
X-ray wavelength (Å)	1.0000	1.4854	1.0000
Space group	$P4_12_12$	$P4_12_12$	$P4_12_12$
Unit-cell parameters (Å)	$a = b = 143.9$,	$a = b = 144.3$,	$a = b = 143.2$,
	$c = 149.8$	$c = 149.6$	$c = 149.5$
Resolution range (Å)	50–2.67 (2.72–2.67)	50–3.95 (4.02–3.95)	50–3.30 (3.36–3.30)
Total/unique reflections	637739/45336	191778/14488	230159/23779
Completeness (%)	100.0 (100.0)	100.0 (100.0)	98.8 (99.5)
Average $I/\sigma(I)$	51.5 (7.9)	38.1 (11.6)	13.1 (4.6)
R_{merge}† (%)	10.3 (56.7)	14.9 (41.6)	19.0 (50.8)
Model-refinement statistics			
Resolution range (Å)	47.19–2.67		47.06–3.42
R_{work}/R_{free}‡ (%)	18.2/20.7		17.3/20.9
No. of atoms			
Protein non-H atoms	5193		5193
Water O atoms	147		14
Average B factors (Å^2)			
Protein non-H atoms	50.16		33.68
Water O atoms	43.31		20.61
R.m.s. deviations from ideal			
Bond lengths (Å)	0.005		0.005
Bond angles (°)	0.909		0.894
Protein geometry analysis			
Ramachandran favoured (%)	94.67		93.93
Ramachandran allowed (%)	5.33		6.07
Ramachandran outliers (%)	0		0

† $R_{merge} = \sum_{hkl} \sum_i |I_i(hkl) - \langle I(hkl) \rangle| / \sum_{hkl} \sum_i I_i(hkl)$, where $I(hkl)$ is the intensity of reflection hkl, $\sum_{hkl}$ is the sum over all reflections and $\sum_i$ is the sum over i measurements of reflection hkl. ‡ $R = \sum_{hkl} ||F_{obs}| - |F_{calc}|| / \sum_{hkl} |F_{obs}|$, where R_{free} was calculated for a randomly chosen 5% of reflections which were not used for structure refinement and R_{work} was calculated for the remaining reflections.

(a)

(b)

(c)

2.7. Phosphodiesterase assay

Phosphodiesterase activity was measured with the artificial chromogenic substrate bis-p-nitrophenyl phosphate (bpNPP) by monitoring the increase in absorbance at 410 nm (Kuznetsova *et al.*, 2005) using an S-3100 spectrophotometer (SCINCO). For metal chelation, the Tm1162 protein was treated with 30 mM EDTA and subsequently desalted with 20 mM Tris–HCl pH 8.0, 200 mM NaCl. The assays included 40 μM bpNPP in a reaction mixture consisting of 25 μM Tm1162, 1 mM metal ions (MnCl$_2$, FeCl$_3$, NiSO$_4$, CuCl$_2$ and/or zinc acetate) and 50 mM Tris–HCl pH 8.0. To determine the K_{m} and k_{cat} values of Tm1162, the reactions were initiated by the addition of a concentrated aliquot of Tm1162 to the reaction solution. The final concentration of Tm1162 ranged from 1.25 to 20 μM.
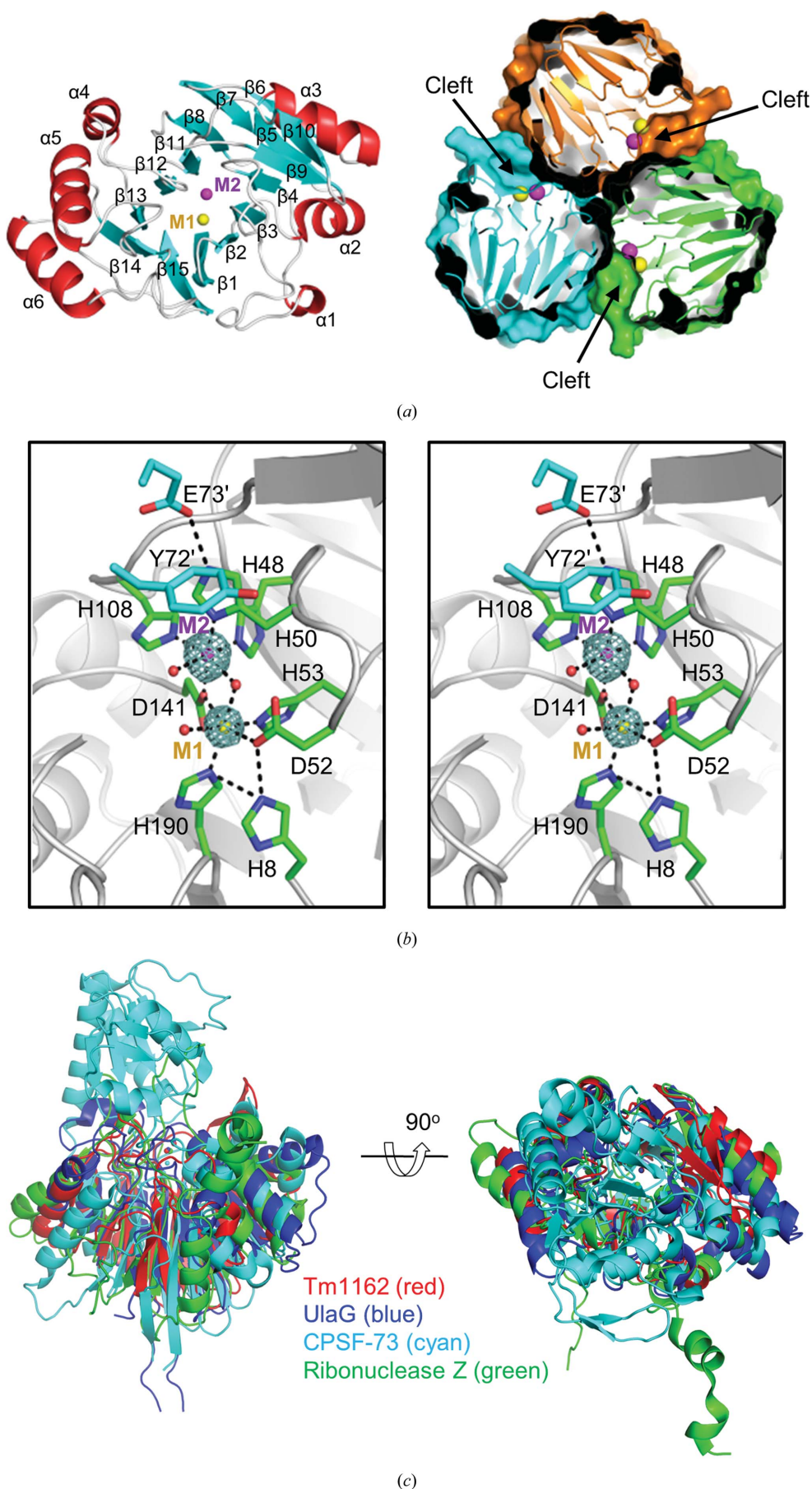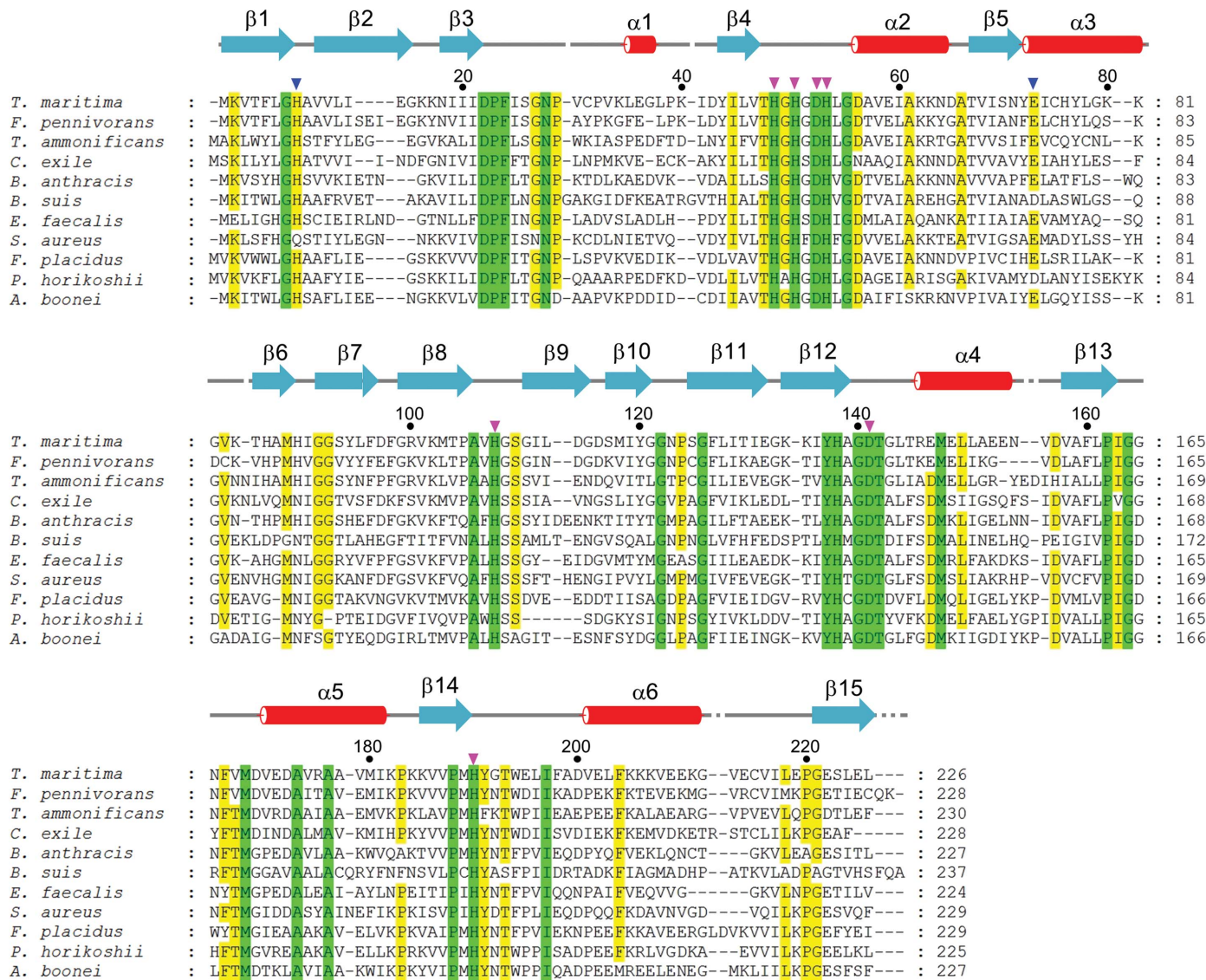
Figure 1
Crystal structure of Tm1162. (*a*) Ribbon diagram of the monomeric structure of Tm1162. Helices and strands are coloured red and cyan, respectively. The two metal ions are coloured yellow (M1) and magenta (M2). All figures were drawn using monomers *A* and *B* in the asymmetric unit. (*b*) Cross-section of the Tm1162 trimeric structure. The three clefts are indicated by arrows. Different subunits are drawn in different colours. (*c*) Stereo diagram of the OMIT map for coordinated metals in Tm1162. The ($F_{\mathrm{o}} - F_{\mathrm{c}}$) difference electron-density map is contoured at 3σ. Primes denote residues from neighbouring subunits. Black dotted lines denote hydrogen bonds. (*d*) Structural comparison of Tm1162 with several hydrolases. Superposition of the structure of Tm1162 (PDB entry 3x30, coloured red) with those of *E. coli* UlaG (PDB entry 2wym, coloured blue), human CPSF-73 (PDB entry 2i7t, coloured cyan) and *B. subtilis* ribonuclease Z (PDB entry 1y44, coloured green).

3. Results and discussion

3.1. The crystal structure of Tm1162 exhibits the metallo-β-lactamase-like fold

The crystal structure of Tm1162 was solved by the multi-wavelength anomalous diffraction method and refined to final R_{work} and R_{free} values of 15.6 and 18.2%, respectively, at a resolution of 1.92 Å (Table 1). The refined model of Tm1162 accounts for residues 1–226 with a cloning artifact (Gly0) in the asymmetric unit and 157 water molecules. Ramachandran plot analysis of the refined model showed that 96.89, 3.11 and 0% of the nonglycine residues are in the most favoured, allowed and disallowed regions, respectively (Table 1; Lovell *et al.*, 2003). The crystal structure of Tm1162 primarily consists of six α-helices and 15 β-strands (Figs. 1*a* and 2), exhibiting the metallo-β-lactamase-like fold (αβ/βα fold) with a core of two β-sheets (β1–β6 and β15, and β7, β8 and β11–β14) flanked on each side by α-helices (Fig. 1*a*). Each of the core β-sheets consists of four antiparallel β-strands followed by three or two parallel β-strands (Fig. 1). The active site (metal-coordination
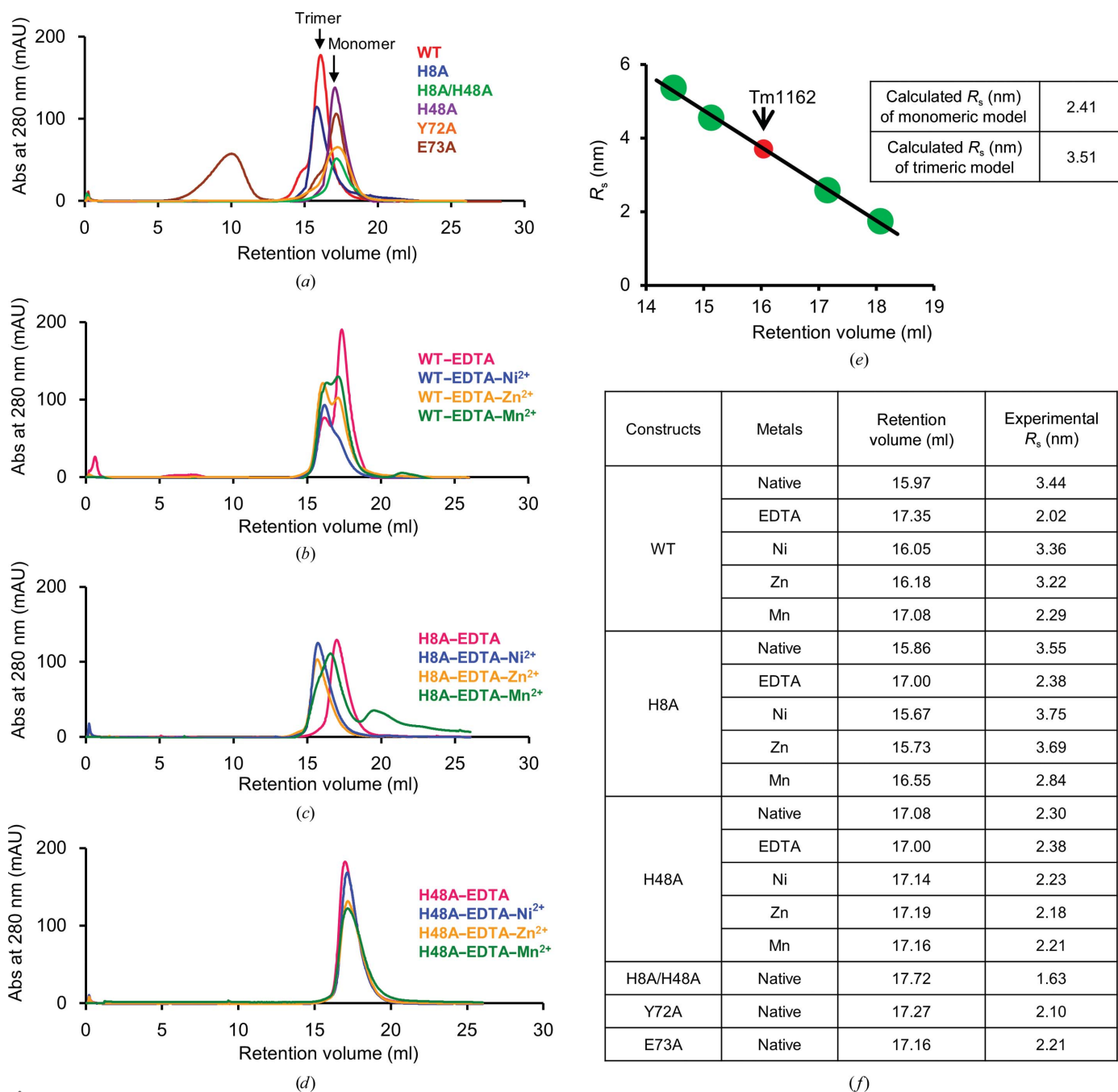

Figure 2
Multiple sequence alignment of Tm1162 (UniProtKB/Swiss-Prot accession No. Q9X0P5) against metal-dependent hydrolases from *Fervidobacterium pennivorans* (UniProtKB/Swiss-Prot accession No. H9UBX9), *Thermovibrio ammonificans* (UniProtKB/Swiss-Prot accession No. E8T4R2), *Caldisericum exile* (UniProtKB/Swiss-Prot accession No. I0GKX1), *Bacillus anthracis* (UniProtKB/Swiss-Prot accession No. Q81KX6), *Brucella suis* (UniProtKB/Swiss-Prot accession No. A9WYR5), *Enterococcus faecalis* (UniProtKB/Swiss-Prot accession No. Q835K6), *Staphylococcus aureus* (UniProtKB/Swiss-Prot accession No. Q6GG00), *Ferroglobus placidus* (UniProtKB/Swiss-Prot accession No. D3RXB0), *Pyrococcus horikoshii* (UniProtKB/Swiss-Prot accession No. O59330) and *Aciduliprofundum booneii* (UniProtKB/Swiss-Prot accession No. B5IDP5). Secondary-structure elements were assigned by *PyMOL* (http://www.pymol.org) and every 20th residue is marked by a black dot. Strictly (100%) and semi-conserved (above 80%) residues are highlighted in green and yellow, respectively. Arrows above the sequences denote α-helices and cylinders denote β-strands. Pink triangles above the sequences indicate the residues that directly coordinate metal ions at the active site and blue triangles denote residues in the second coordination sphere.

site) of Tm1162 is located at the edge of the core β-sheets and contains two metal ions (M1 and M2; Figs. 1b and 1c).

A structural similarity search for Tm1162 using the *DALI* server (Holm & Rosenström, 2010) identified several kinds of hydrolase structures: L-ascorbate-6-phosphate lactonases, cleavage and polyadenylation specificity factors (CPSF) and ribonucleases. The L-ascorbate-6-phosphate lactonase UlaG from *E. coli* (PDB entry 2wym; Garces *et al.*, 2010), human CPSF-73 (PDB entry 2i7t; Mandel *et al.*, 2006) and

ribonuclease Z from *Bacillus subtilis* (PDB entry 1y44; Li de la Sierra-Gallay *et al.*, 2005) align with Tm1162 with Z-scores (normalized statistical similarity weights) of 25.0, 21.7 and 21.0 (r.m.s.d.s of 2.1, 2.5 and 2.7 Å for 214, 202 and 203 C$^\alpha$ atoms; Fig. 1d), respectively. This suggests that their overall monomer structures are similar. Similar to Tm1162, these structures also exhibit an $\alpha\beta/\beta\alpha$ fold with metal-coordination sites located at the end of the β-sheet sandwich (Fig. 1d).

Figure 3
Analytical gel filtration of wild-type Tm1162 and its mutants. (a) Analytical gel-filtration profiles of wild-type and mutants of Tm1162. (b, c, d) Analytical gel-filtration profiles of EDTA-treated wild-type (b), H8A mutant (c) and H48A mutant (d) Tm1162 in the presence of the indicated metal ions. (e) Standard curve using molecular-weight markers. The positions of the molecular-weight markers (β-amylase, alcohol dehydrogenase, carbonic anhydrase and cytochrome c) are indicated with green dots. The position of Tm1162 is marked with a red dot. (f) Values of the retention volume and Stokes radius (R_s) determined by the analytical gel-filtration experiments shown in this figure.
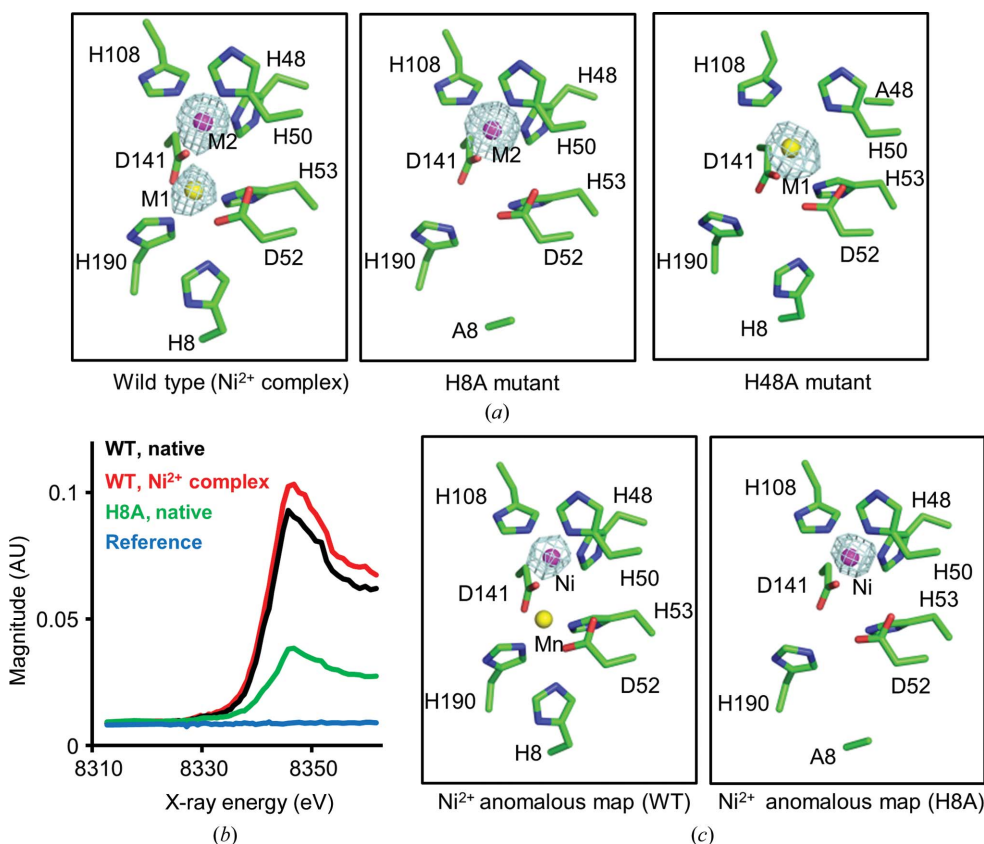
Constructs	Metals	Retention volume (ml)	Experimental R_s (nm)
WT	Native	15.97	3.44
	EDTA	17.35	2.02
	Ni	16.05	3.36
	Zn	16.18	3.22
	Mn	17.08	2.29
H8A	Native	15.86	3.55
	EDTA	17.00	2.38
	Ni	15.67	3.75
	Zn	15.73	3.69
	Mn	16.55	2.84
H48A	Native	17.08	2.30
	EDTA	17.00	2.38
	Ni	17.14	2.23
	Zn	17.19	2.18
	Mn	17.16	2.21
H8A/H48A	Native	17.72	1.63
Y72A	Native	17.27	2.10
E73A	Native	17.16	2.21

(f)

Table 3
Metal-binding interactions.

Residue	Metal	Distance (Å)		
		Wild type	Wild type–nickel	H8A
His48 (NE2)	M2	2.2	2.4	2.5
His50 (ND1)	M2	2.2	2.4	2.3
His108 (NE2)	M2	2.1	2.2	2.3
Asp141 (OD2)	M2	2.1	2.2	2.2
H$_2$O 127 (O)	M2	2.2		
H$_2$O 126 (O)	M2	2.2		
Asp141 (OD2)	M1	2.1	2.1	
His53 (NE2)	M1	2.2	2.6	
Asp52 (OD2)	M1	2.4	2.5	
His190 (NE2)	M1	2.3	2.4	
H$_2$O 159 (O)	M1	2.4		
H$_2$O 126 (O)	M1	2.2		

3.2. The active site is formed at the interface between two monomers of the trimer

Although one monomer of Tm1162 is present in the asymmetric unit, a possible trimer could be generated by crystallographic threefold symmetry (Fig. 1b). The trimer is globular, with approximate dimensions of 70 × 70 × 50 Å (Fig. 1b). The solvent-accessible surface area buried at the interface between two monomers in the trimeric unit is ~1000 Å^2 (~20% of the monomer surface area), suggesting that Tm1162 may exist in solution as the trimer that is present in the crystal (Krissinel & Henrick, 2007). To analyze the quaternary structure of Tm1162 in solution, analytical gel filtration was performed using a Superdex 200 (10/300 GL) column (Fig. 3). The Stokes radius of Tm1162 was estimated to be 3.51 nm, which is highly similar to the calculated Stokes radius (3.75 nm) of the Tm1162 trimer (Fig. 3e). This result strongly suggests that Tm1162 primarily exists in solution as the trimer present in the crystal. To determine whether there are similar trimer structures in the MBL superfamily, the *DALI* server was used to determine similar fold structures; however, no trimeric assembly like Tm1162 was found. This indicates that the Tm1162 trimer is an uncharacterized quaternary structure in the MBL superfamily.

Three narrow clefts are present around the interface between the two monomers, in which the active sites and metal-coordination sites are present (Fig. 1b). Oligomerization is expected to be essential for the activity of Tm1162 because the active site is formed at the interface between two monomers of the trimer (Fig. 1b). An interdomain hydrogen bond (2.8 Å) between the OE2 atom of Glu73′ (where the prime indicates that the residue belongs to a neighbouring subunit) and the NE2 atom of His50 maintains the orientation of the His50 imidazole ring. This suggests that the neighbouring subunit contributes to the proper orientation of the active-site residues that make direct contacts with the M2 ion (Fig. 1c).

3.3. Novel second coordination sphere of the nickel-containing heterodinuclear site

Strong electron densities for two metal ions (M1 and M2) were found in the OMIT map of each Tm1162 subunit (Figs. 1c and 4). In the structure of Tm1162, the distance between a pair of dimetal centres in the trimer is ~25 Å, indicating that the three active sites within the trimer are well separated and that they can function independently. In the dimetal centre of Tm1162, the distance between the two metal ions is 3.4 Å. M1 binds to Asp52 (OD2 atom), His53 (NE2 atom), Asp141 (OD2 atom) and His190 (NE2 atom) with distances of 2.4, 2.2, 2.1 and 2.3 Å, respectively. M2 binds to His48 (NE2 atom),

Figure 4
OMIT and anomalous difference Fourier maps of wild-type and mutants of Tm1162. (a) OMIT electron-density map for metal ions for the nickel complex, the H8A mutant and the H48A mutant of Tm1162 are shown in mesh. The ($F_o − F_c$) difference electron density is contoured at 5σ. (b) X-ray absorption spectra of the nickel ions in the wild type (black), the nickel complex (red) and the H8A mutant (green) of Tm1162. (c) Anomalous difference Fourier maps illustrating the positions of Ni^{2+} for the wild type and the H8A mutant of Tm1162 are shown in mesh. The ($F_o − F_c$) difference electron density is contoured at 8σ.

Table 4
Steady-state kinetic values of wild-type Tm1162 and mutants.

Substrate	Tm1162	K_m (μM)	k_{cat} (s^{-1})	k_{cat}/K_m (M^{-1} s^{-1})
Nitrocefin	Wild type (Ni^{2+} + Mn^{2+})	0.39 ± 0.01	98.4 ± 0.3	25 × 10^7
	Wild type (EDTA)	1.47 ± 0.06	110.0 ± 1.2	7.5 × 10^7
	H8A	1.30 ± 0.05	108.1 ± 0.8	8.3 × 10^7
	H48A	1.09 ± 0.04	106.3 ± 1.1	9.8 × 10^7
	H8A/H48A	1.45 ± 0.03	109.7 ± 1.2	7.6 × 10^7
bpNPP	Wild type (Ni^{2+} + Mn^{2+})	23.7 ± 0.2	41.6 ± 0.2	1.8 × 10^3

His50 (NE2 atom), His108 (NE2 atom) and Asp141 (OD2 atom) with distances of 2.2, 2.2, 2.1 and 2.1 Å, respectively (Fig. 1c). The observed metal coordinations at the dimetal site of Tm1162 were distinct from those of MBL family proteins in the second coordination sphere. Notably, the NE2 atom of His8, which resides near the active site but does not make a direct contact with the M1 ion, forms hydrogen bonds to

Asp52 (OD2 atom) and His190 (NE2 atom) with distances of 2.7 and 3.1 Å, respectively (Fig. 1c). The second coordination sphere generally stabilizes the conformational orientations of the active-site residues and enhances the metal affinity (Dudev & Lim, 2014). Given this, we hypothesized that the two hydrogen bonds between His8 and Asp52 (or His190) contribute to metal-ion coordination indirectly. Metal-binding interactions are listed in Table 3.

3.4. Crystal structure determination of Tm1162 mutants (H8A and H48A)

To further evaluate the contribution of His8 to M1 ion coordination, the crystal structure of the Tm1162 H8A mutant was solved (Fig. 4a, middle panel). The OMIT $2F_o − F_c$ map of the M1 site disappeared compared with that of wild-type Tm1162 (Fig. 4a, left panel), demonstrating the crucial role of His8 in maintaining the orientations of Asp52 and His190, which are coordinated to M1. To evaluate the contribution of His48 to M2 ion coordination, the crystal structure of the Tm1162 H48A mutant was also solved (Fig. 4a, right panel). The OMIT $2F_o − F_c$ map of the M2 site disappeared compared with that of wild-type Tm1162 (Fig. 4a, left panel), demonstrating the crucial role of His48 in M2 coordination. The monomer structures of the H8A and H48A mutants are virtually identical, with r.m.s. deviations of 1.3 and 0.3 Å for 224 C$^\alpha$ atoms, respectively. We conclude that the H8A and H48A mutations of Tm1162 abolish the binding of metals to the M1 and M2 sites, respectively.

3.5. Characterization of the nickel-binding site

Most proteins in the MBL family contain a conserved metal-coordination site at the edge of two β-sheets (Fig. 5). However, to date there has been no experimental observation of a catalytically essential nickel-containing dinuclear centre at the active site of any protein in the MBL superfamily. As the X-ray absorption spectra of the wild-type (black), nickel complex (red) and H8A mutant (green) of Tm1162 indicated the presence of nickel ions (Fig. 4b), we hypothesized that Tm1162 contains at least one nickel site between the two metal sites. To explore the location of the nickel-binding site, the anomalous difference Fourier map was calculated using data collected at the high-energy side of the nickel absorp-
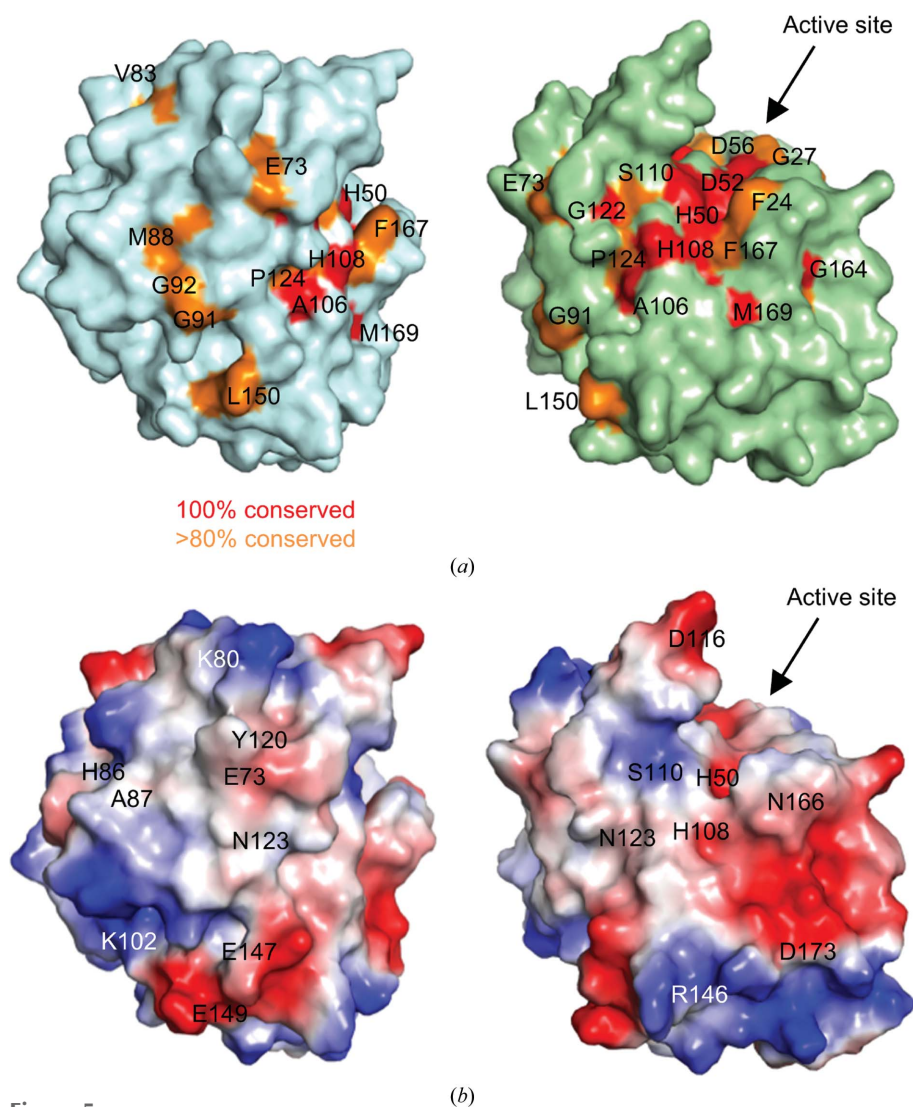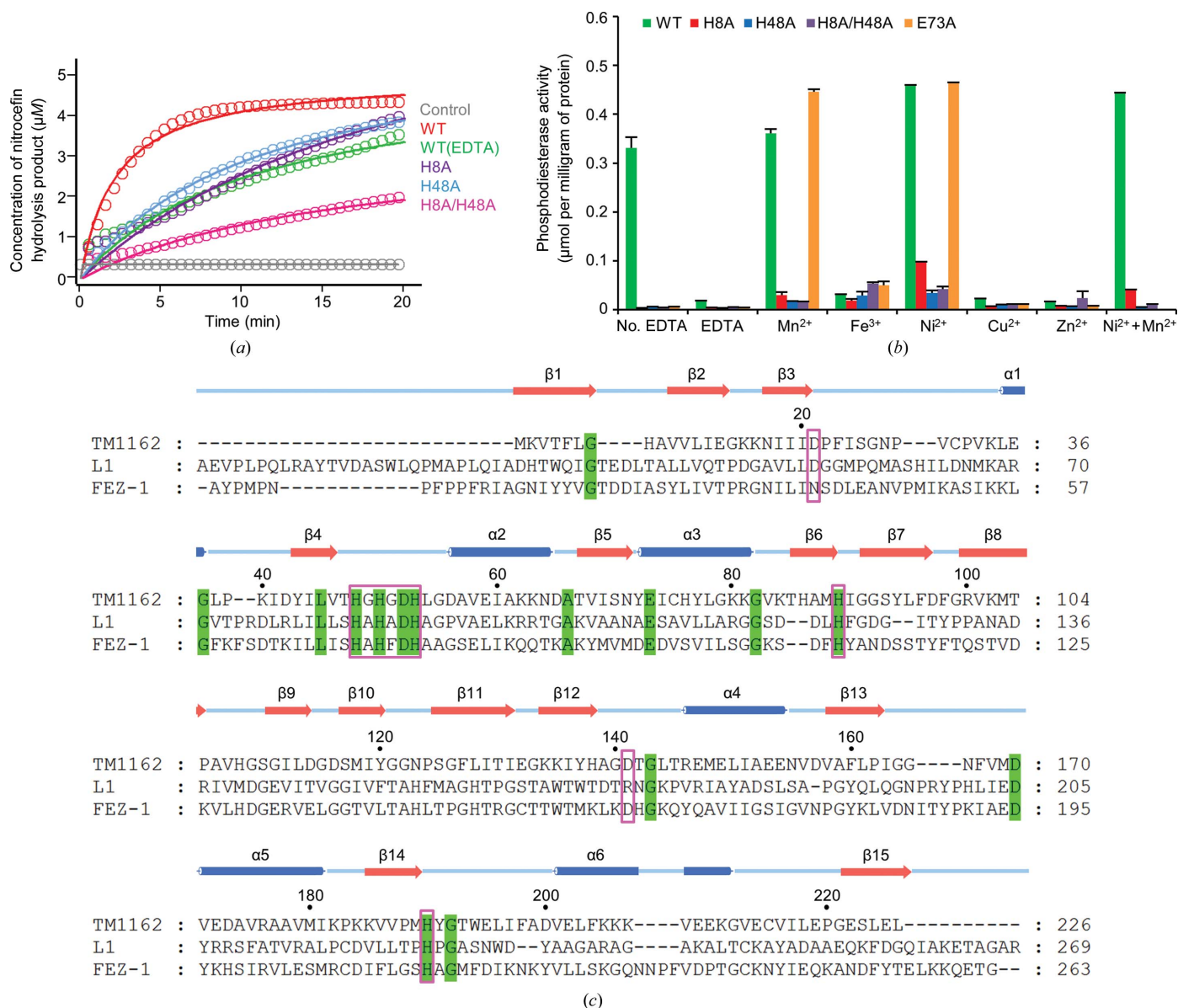

Figure 5
Surface representation of the sequence conservation and electrostatic potential of Tm1162. (a) Sequence conservation mapped onto the surface of the Tm1162 oligomer interface. The conserved residues are coloured red (100%) and orange (greater than 80%). (b) The surface of the Tm1162 oligomer interface is coloured according to the electrostatic potential.

tion peak, which shows three strong peaks (Figs. 4b and 4c). The strong peaks are associated with M2 at the three active sites of the trimer (Fig. 4c, left panel). The nickel anomalous difference Fourier map of the Tm1162 H8A mutant also showed strong peaks at the M2 site of all three subunits (Fig. 4c, right panel), demonstrating that the identity of M2 atom is nickel. We incorporated Mn^{2+} into the M1 sites of Tm1162 for the following reasons. Firstly, Tm1162 showed a significant phosphodiesterase activity in the presence of manganese ions, which was comparable to that with Ni^{2+} (Fig. 6b). Secondly, an inductively coupled plasma mass-spectrometric (ICP-MS) analysis indicated the presence of Mn^{2+} in Tm1162. Thirdly,

Mn^{2+} fits well to the weaker electron density of M1 compared with that of the M2 site (Fig. 1c).

3.6. Metal-dependent oligomerization of Tm1162

We next sought to determine whether the oligomerization of Tm1162 is metal-dependent. As the metal-coordination sites reside at the interfaces between two monomers (Fig. 1b), we hypothesized that Ni^{2+} or Mn^{2+} could play a crucial role in Tm1162 oligomerization. To analyze the possible metal-dependent oligomerization of Tm1162, the quaternary structures of various Tm1162 mutants were determined by analy-

Figure 6
β-Lactamase and phosphodiesterase activities of Tm1162. (a) β-Lactamase assay of Tm1162. The activities are quantified using the hydrolysis of the β-lactamase substrate nitrocefin. (b) Phosphodiesterase assay of Tm1162 and its mutants. The metal-dependent activities are quantified using the hydrolysis of the artificial substrate bpNPP. Phosphodiesterase activities are expressed as micromoles of *p*-nitrophenol per milligram of protein. (c) Sequence alignment of Tm1162 and MBL superfamily subclass B3 proteins: L1 from *Stenotrophomonas maltophilia* (UniProtKB/Swiss-Prot accession No. P52700) and FEZ-1 from *Fluoribacter gormanii* (UniProtKB/Swiss-Prot accession No. Q9K578). Five conserved motifs are boxed in magenta. Conserved residues are highlighted in green. Arrows above the sequences denote α-helices and cylinders denote β-strands.

tical gel filtration (Fig. 3). Interestingly, the H8A mutant, which affects the M1 site, migrated as a trimer (*i.e.* similar to the wild-type protein). However, those mutants that affect the M2 site (H48A, H8A/H48A, Y72A and E73A) migrated as monomers (Fig. 3*a*). This indicates that the M2 site is crucial for the oligomerization of Tm1162. EDTA treatment of the wild-type protein changed the trimeric form into the monomeric form, and this process was reversed by subsequent metal binding (Ni^{2+}, Zn^{2+} and Mn^{2+}; Fig. 3*b*). Similar behaviour was observed with the H8A mutant, which affects the M1 site, upon EDTA treatment and subsequent metal binding (Fig. 3*c*). However, the H48A mutant that affects the M2 site migrated as a monomer upon EDTA treatment and subsequent metal binding, demonstrating the crucial role of M2 site for oligomerization of Tm1162 (Fig. 3*d*). This indicates that the M1 site is not crucial for the oligomerization of Tm1162.

3.7. Tm1162 has β-lactamase activity

Given that the overall fold of Tm1162 belongs to the MBL superfamily, we hypothesized that the signature motifs of β-lactamases would be embedded in the Tm1162 protein sequence (Fig. 6*c*). When the sequence of Tm1162 was aligned with those of the four classes of β-lactamase (A–D; Bebrone, 2007), Tm1162 was found to contain signature motifs that were similar to those of the subclass B3 β-lactamases (Fig. 6*c*), raising the possibility that Tm1162 may possess β-lactamase activity. Based on this sequence analysis, we checked whether Tm1162 had the ability to cleave a β-lactam structure, using nitrocefin as the substrate. Indeed, the wild-type Tm1162 showed β-lactamase activity against the substrate nitrocefin (Fig. 6*a*). The β-lactamase activity of Tm1162 was significantly inhibited by EDTA or an H8A mutation at the active site, showing that the observed β-lactamase activity is clearly an inherent property of Tm1162 and is not owing to contaminating β-lactamases (Fig. 6*a*). Tm1162 possesses a lower K_m value for nitrocefin (Table 4) than other β-lactamases such as GIM-1, IMP-1, VIM-1, VIM-2 and SPM1 (Walsh *et al.*, 2005), implying a tighter binding of the β-lactam moiety of nitrocefin.

3.8. Tm1162 has metal-dependent phosphodiesterase activity

Several hits with high Z-scores from the *DALI* server include ribonucleases such as ribonuclease Z from *B. subtilis* (PDB entry 1y44), and the active site of Tm1162 is similar to that of a ribonuclease (Fig. 1*c*). Given this information, we hypothesized that Tm1162 may possess phosphodiesterase activity. Phosphodiesterase assays with Tm1162 were performed using bis-(*p*-nitrophenyl)phosphate (bpNPP), a general substrate for phosphodiesterases, with several buffers containing different metal ions. Indeed, the wild-type Tm1162 showed phosphodiesterase activity (Fig. 6*b*). The phosphodiesterase activity was abolished by treatment with EDTA, indicating that the activity is metal-dependent (Fig. 6*b*). In the presence of Ni^{2+}, Tm1162 showed the highest phosphodiesterase activity towards bpNPP, while its phosphodiesterase activity was reduced in the presence of manganese ions (Fig. 6*b*). Tm1162 displayed negligible phosphodiesterase

activity with other metal ions (Fe^{3+}, Cu^{2+} and Zn^{2+}), suggesting that this protein selectively requires Ni^{2+} or Mn^{2+} ions for phosphodiesterase activity. Mutations at the active site (H8A, H48A and H8A/H48A) abolished the phosphodiesterase activity. This illustrates that the observed phosphodiesterase activity is clearly an inherent property of Tm1162 and is not owing to contaminating phosphodiesterases (Fig. 6*b*). We hypothesized that mutation of Glu73′ might affect the catalytic activity of Tm1162, as Glu73′ contributes indirectly to the formation of the active site at the monomer–monomer interface. Indeed, an E73A mutation abolished the phosphodiesterase activity, suggesting that oligomerization is essential for the phosphodiesterase activity of Tm1162 (Fig. 6*b*). The K_m value for bpNPP in the phosphodiesterase activity ($23.7 \pm 0.2\ \mu M$) was higher than that for nitrocefin in the β-lactamase activity ($0.39 \pm 0.01\ \mu M$) (Table 4).

4. Conclusion

As an array of metal ions with varying concentrations is available inside cells, selective binding of metal ions with high fidelity is crucial for the function of metalloproteins. In an effort to understand the structural mechanism that governs metal selectivity, we have identified a new type of structurally encoded nickel-containing heterodinuclear site in Tm1162, which belongs to the β-lactamase B3 subclass. The active site of Tm1162 showed several novel features compared with other proteins of the MBL family. Firstly, the active site is formed at the interface between two monomers of a trimer, which is an uncharacterized quaternary structure in the MBL superfamily. Secondly, the second coordination sphere (His8 and Glu73′) of the nickel-containing heterodinuclear site contributes to the specificity of nickel-ion binding. Thirdly, the M2 site is not only crucial for the β-lactamase and phosphodiesterase catalytic activities, but also for the oligomerization of Tm1162.

Antibiotics containing the β-lactam moiety are some of the major antimicrobial agents. The emergence of antibiotic resistance among human bacterial pathogens is a significant public health concern (Feng *et al.*, 2014; Palzkill, 2013). Accordingly, β-lactamases have attracted much attention as targets for the development of new antibiotics. In this study, we have solved the crystal structure of Tm1162, a metallo-β-lactamase, which reveals unique aspects such as an uncharacterized quaternary structure, a nickel-containing active site and nickel-dependent oligomerization. The unique features of the Tm1162 structure might help in the design of a novel class of antibiotics targeting β-lactamases similar to Tm1162. Broadly, the structural and functional studies of Tm1162 described here could be adapted to other unknown proteins, which may facilitate the identification of nickel-containing metalloenzymes that mimic the nickel-containing heterodinuclear site of Tm1162. Although much remains to be learned about the structural mechanisms that govern metal selectivity and nickel selectivity, the results and model presented here provide one foothold for furthering such understanding.

research papers

References

Adams, P. D., Grosse-Kunstleve, R. W., Hung, L.-W., Ioerger, T. R., McCoy, A. J., Moriarty, N. W., Read, R. J., Sacchettini, J. C., Sauter, N. K. & Terwilliger, T. C. (2002). *Acta Cryst.* D**58**, 1948–1954.

Bebrone, C. (2007). *Biochem. Pharmacol.* **74**, 1686–1701.

Boer, J. L., Mulrooney, S. B. & Hausinger, R. P. (2014). *Arch. Biochem. Biophys.* **544**, 142–152.

Bushnell, G. W., Louie, G. V. & Brayer, G. D. (1990). *J. Mol. Biol.* **214**, 585–595.

Cheong, C. G., Eom, S. H., Chang, C., Shin, D. H., Song, H. K., Min, K., Moon, J. H., Kim, K. K., Hwang, K. Y. & Suh, S. W. (1995). *Proteins*, **21**, 105–117.

Christianson, D. W. & Cox, J. D. (1999). *Annu. Rev. Biochem.* **68**, 33–57.

Dudev, T. & Lim, C. (2014). *Chem. Rev.* **114**, 538–556.

Eidam, O., Romagnoli, C., Dalmasso, G., Barelier, S., Caselli, E., Bonnet, R., Shoichet, B. K. & Prati, F. (2012). *Proc. Natl Acad. Sci. USA*, **109**, 17448–17453.

Emsley, P. & Cowtan, K. (2004). *Acta Cryst.* D**60**, 2126–2132.

Fast, W. & Sutton, L. D. (2013). *Biochim. Biophys. Acta*, **1834**, 1648–1659.

Feng, H., Ding, J., Zhu, D., Liu, X., Xu, X., Zhang, Y., Zang, S., Wang, D.-C. & Liu, W. (2014). *J. Am. Chem. Soc.* **136**, 14694–14697.

Fisher, J. F., Meroueh, S. O. & Mobashery, S. (2005). *Chem. Rev.* **105**, 395–424.

Garces, F., Fernández, F. J., Montellà, C., Penya-Soler, E., Prohens, R., Aguilar, J., Baldomà, L., Coll, M., Badia, J. & Vega, M. C. (2010). *J. Mol. Biol.* **398**, 715–729.

García de la Torre, J., Huertas, M. L. & Carrasco, B. (2000). *Biophys. J.* **78**, 719–730.

Heinz, U. & Adolph, H.-W. (2004). *Cell. Mol. Life Sci.* **61**, 2827–2839.

Holm, L. & Rosenström, P. (2010). *Nucleic Acids Res.* **38**, W545–W549.

Hu, Z., Spadafora, L. J., Hajdin, C. E., Bennett, B. & Crowder, M. W. (2009). *Biochemistry*, **48**, 2981–2989.

Krissinel, E. & Henrick, K. (2007). *J. Mol. Biol.* **372**, 774–797.

Kuznetsova, E., Proudfoot, M., Sanders, S. A., Reinking, J., Savchenko, A., Arrowsmith, C. H., Edwards, A. M. & Yakunin, A. F. (2005). *FEMS Microbiol. Rev.* **29**, 263–279.

Li de la Sierra-Gallay, I., Pellegrini, O. & Condon, C. (2005). *Nature (London)*, **433**, 657–661.

Lovell, S. C., Davis, I. W., Arendall, W. B., de Bakker, P. I. W., Word, J. M., Prisant, M. G., Richardson, J. S. & Richardson, J. S. (2003). *Proteins*, **50**, 437–450.

Mandel, C. R., Kaneko, S., Zhang, H., Gebauer, D., Vethantham, V., Manley, J. L. & Tong, L. (2006). *Nature (London)*, **444**, 953–956.

McCoy, A. J., Grosse-Kunstleve, R. W., Adams, P. D., Winn, M. D., Storoni, L. C. & Read, R. J. (2007). *J. Appl. Cryst.* **40**, 658–674.

Mulrooney, S. B. & Hausinger, R. P. (2003). *FEMS Microbiol. Rev.* **27**, 239–261.

Neuwald, A. F., Liu, J. S., Lipman, D. J. & Lawrence, C. E. (1997). *Nucleic Acids Res.* **25**, 1665–1677.

Otwinowski, Z. & Minor, W. (1997). *Methods Enzymol.* **276**, 307–326.

Palzkill, T. (2013). *Ann. N. Y. Acad. Sci.* **1277**, 91–104.

Pérez-Llarena, F. J. & Bou, G. (2009). *Curr. Med. Chem.* **16**, 3740–3765.

Punta, M. *et al.* (2011). *Nucleic Acids Res.* **40**, D290–D301.

Quiroga, M. I., Franceschini, N., Rossolini, G. M., Gutkind, G., Bonfiglio, G., Franchino, L. & Amicosante, G. (2000). *Chemotherapy*, **46**, 177–183.

Ragsdale, S. W. (2009). *J. Biol. Chem.* **284**, 18571–18575.

Raj, S. B., Ramaswamy, S. & Plapp, B. V. (2014). *Biochemistry*, **53**, 5791–5803.

Saito, R., Sato, T., Ikai, A. & Tanaka, N. (2004). *Acta Cryst.* D**60**, 792–795.

Sheffield, P., Garrard, S. & Derewenda, Z. (1999). *Protein Expr. Purif.* **15**, 34–39.

Terwilliger, T. C. (2003). *Methods Enzymol.* **374**, 22–37.

The UniProt Consortium (2013). *Nucleic Acids Res.* **41**, D43–D47.

Walsh, T. R., Toleman, M. A., Poirel, L. & Nordmann, P. (2005). *Clin. Microbiol. Rev.* **18**, 306–325.

Wang, Z. & Benkovic, S. J. (1998). *J. Biol. Chem.* **273**, 22402–22408.

Winn, M. D. *et al.* (2011). *Acta Cryst.* D**67**, 235–242.